Solin, Katariina; Beaumont, Marco; Rosenfeldt, Sabine; Orelma, Hannes; Borghei, Maryam; Bacher, Markus; Opietnik, Martina; Rojas, Orlando J.

Self-Assembly of Soft Cellulose Nanospheres into Colloidal Gel Layers with Enhanced Protein Adsorption Capability for Next-Generation Immunoassays

Published in:
Small

DOI:
10.1002/smll.202004702

Published: 17/12/2020

Document Version
Publisher's PDF, also known as Version of record

NANO · MICRO small
www.small-journal.com

Self-Assembly of Soft Cellulose Nanospheres into Colloidal Gel Layers with Enhanced Protein Adsorption Capability for Next-Generation Immunoassays

Katariina Solin, Marco Beaumont, Sabine Rosenfeldt, Hannes Orelma, Maryam Borghei, Markus Bacher, Martina Opietnik, and Orlando J. Rojas**

Soft cationic core/shell cellulose nanospheres can deform and interpenetrate allowing their self-assembly into densely packed colloidal nanogel layers. Taking advantage of their water-swelling capacity and molecular accessibility, the nanogels are proposed as a new and promising type of coating material to immobilize bioactive molecules on thin films and paper. The specific and nonspecific interactions between the cellulosic nanogel and human immunoglobulin G as well as bovine serum albumin (BSA) are investigated. Confocal microscopy, electroacoustic microgravimetry, and surface plasmon resonance are used to access information about the adsorption behavior and viscoelastic properties of self-assembled nanogels. A significant BSA adsorption capacity on nanogel layers (17 mg m^{-2}) is measured, 300% higher compared to typical polymer coatings. This high protein affinity further confirms the promise of the introduced colloidal gel layer, in increasing sensitivity and advancing a new generation of substrates for a variety of applications, including immunoassays, as demonstrated in this work.

1. Introduction

Cellulose can be regarded as one of nature's best examples of structural polymers with abundant surface hydroxyl groups and a remarkable elastic modulus, in the range of 138–220 GPa for cellulose crystals.[1,2] This explains the high interest on the rigid, rod-like cellulose nanocrystals (CNC) obtained via acidic hydrolysis of cellulose fibers.[3] However, the potential of functional soft, core–shell cellulosic nanoparticles, for instance, to alter surface activity toward proteins,[4,5] remains largely untapped. Nanoparticles are generally synthesized by grafting soft polymeric structures onto rigid, rod-like nanocrystals, i.e., becoming hard-core/soft-shell nanoparticles.[6,7] This approach is rather time-consuming, especially if compared to cellulose II hydrogels.[8–10] Expanding on the latter, cellulose II nanospheres have been recently introduced through a facile and "green" avenue.[11,12] They consist of spherical nanocrystals[13–15] interconnected within a fibrillar network.[8–10,16] By installing repulsive charges onto the surface of cellulose II hydrogels, it is possible to develop functional cellulose II nanospheres with an intrinsic soft and amorphous shell.[11,12] This new class of cellulose colloids features the rheological and electrophoretic properties typical of soft particles as well as intraparticle and pH-responsive swelling behavior. The shells of the soft particles are anionic and can deform and interpenetrate[17–19] into a jammed colloidal nanogel.[12] Among the latter, classical supramolecular nanogels are defined as swollen nanosized networks of polymer chains[20] and are already used, for example, to control protein interactions.[21–24] Controlling these interactions is crucial in

K. Solin, Dr. M. Beaumont, Dr. M. Borghei, Prof. O. J. Rojas
Department of Bioproducts and Biosystems
School of Chemical Engineering
Aalto University
Vuorimiehentie 1, Espoo FI-00076, Finland
E-mail: marcobeaumont1@gmail.com; orlando.rojas@ubc.ca

Dr. M. Beaumont, Dr. M. Bacher
Department of Chemistry
Institute of Chemistry for Renewable Resources
University of Natural Resources and Life Sciences Vienna (BOKU)
Konrad-Lorenz-Strasse 24, Tulln A-3430, Austria

The ORCID identification number(s) for the author(s) of this article can be found under https://doi.org/10.1002/smll.202004702.

DOI: 10.1002/smll.202004702

Dr. S. Rosenfeldt
Bavarian Polymer Institute and Department of Chemistry
University of Bayreuth
Bayreuth D-95440, Germany

Dr. H. Orelma
VTT – Technical Research Centre of Finland
Tietotie 4E, P.O. Box 1000, Espoo FI-02044, Finland

Dr. M. Opietnik
Lenzing AG
Werkstrasse 2, Lenzing A-4860, Austria

Prof. O. J. Rojas
The Bioproducts Institute
Department of Chemical and Biological Engineering
and Department of Chemistry and Wood Science
University of British Columbia
2360 East Mall, Vancouver, BC V6T 1Z4, Canada

diagnostics, tissue engineering, and other biomedical fields[25–27] and has provoked considerable interest in related communities.[21–24,28–33] In general, the affinity of proteins to a surface depends on ionic, electrosteric, hydrogen bonding, and hydrophobic interactions.[34] Meanwhile, the first two types of interactions are associated with protein charge, which is dependent on the protein's isoelectric point and environment pH.[35] In the case of cellulose, related interactions have been mainly tailored through adsorption of soluble polymers.[28,29,31–33] However, a current limitation is that the adsorption of soluble macromolecules occurs not only on the surface of the substrate but also in voids, which may not be accessible to biopolymers or particles. Apart from soluble polymers, adsorption of bovine serum albumin (BSA) is enhanced by using cationic, rigid cellulose nanocrystals. Unfortunately, protein adsorption is, in this case, limited to the crystalline surface of cellulose nanocrystals and this is expected to be significantly lower than in the case of soft nanoparticles.

In this work, we introduce cationic, soft cellulose II nanospheres (NPcat) that spontaneously assemble and are immobilized into a colloidal nanogel layer. Associated processes are monitored using electromechanical (quartz crystal microbalance with dissipation monitoring, QCM-D) and optical (surface plasmon resonance, SPR) sensing. The NPcat nanogel layer is used as a powerful anchor for specific and nonspecific protein adsorption. More specifically, its interactions with BSA and human immunoglobulin G (hIgG) are studied (QCM-D and confocal microscopy), and directly compared to more traditional polymer-coated surfaces. The introduced nanogel layer is demonstrated to trigger protein–surface interactions that can be suitably used in numerous applications.

2. Results and Discussion

NPcat was obtained analogously to our recently reported method.[11,12] It includes a top-down approach from industrially produced cellulose II hydrogels.[10,36] An alternative approach involves a bench-scale procedure based on caustic treatment of microcrystalline cellulose.[8,9] The highly porous structure of the cellulose II material and its nanofibrillar network is shown in **Figure 1**A.

The nanostructured cellulose II hydrogel[10,36] was reacted with glycidyltrimethylammonium chloride in an organic solvent-free process. The conditions were deliberately chosen to allow selective surface modification of the chemically accessible regions of the dispersed cellulose in water (i.e., heterogeneous conditions). The crystalline structure of the cellulose II was not affected through this modification, as shown in the diffractograms included in Figure S1 (Supporting Information). Successful incorporation of the cationic moieties was proven through infrared spectroscopy (Figure S2A, Supporting Information) by the presence of the C—N stretching vibration at 1480 cm^{-1},[37] and a degree of substitution of 0.17 was determined by NMR spectroscopy (Figure S2B, Supporting Information). The introduction of the cationic, repulsive charges onto the amorphous regions of the cellulose II hydrogel, enabled the extraction of spherical NPcat through mechanical shearing in a microfluidizer, as shown in the atomic force microscope (AFM) image (Figure 1B). NPcat featured a particle diameter of 30 ± 8 nm (AFM in air) and a number-averaged hydrodynamic radius of 55 ± 8 nm, obtained from dynamic light scattering (DLS) analysis in 5×10^{-3} M phosphate buffer at pH = 7. The electrophoretic mobility of the particles was measured to be 2.3 ± 0.6 μm cm V^{-1} s^{-1} (5×10^{-3} M NaCl). These values are comparable to those of soft cellulose II nanospheres that were previously reported[12] and used here as a reference (Table S1, Supporting Information). The number of cationic surface groups of the prepared NPcat was 0.9 mmol g^{-1}. Noteworthy, AFM overestimates the particle core diameter of the cellulose II nanospheres, which is ≈16 nm.[12] This is due to the contribution of the particle shell in the measurement. Using a set of characterization methods, including DLS and X-ray diffraction, we showed that NPcat is similar to the reference (Figures S1 and S3, Supporting Information), and features an intrinsic core/shell structure consisting of a densely packed, crystalline core surrounded by a less crystalline and water-swellable soft shell.[12]

Although the soft cellulose II nanospheres feature a repulsive surface charge, they tend to interact with each other forming a nanogel at a gel point of 4 wt% through particle-shell overlap and interpenetration.[12] We, therefore, hypothesize that upon adsorption on an oppositely charged substrate, the colloids interpenetrate with each other, forming a nanogel layer. To study this process, we studied the adsorption of NPcat on ultrathin films of CNF using QCM-D and with SPR. Figures 1C,D shows that compared to a soluble cationic polymer (Figure S4, Supporting Information, and **Table 1**), a considerably larger amount of NPcat was adsorbed on CNF films. The strong affinity of NPcat with the surface is most likely related to electrostatic interactions. This is given by the slight anionic charge of CNF due to the presence of negatively charged hemicelluloses.[38,39] Furthermore, van der Waals forces and entropic effects (counterion release) influence the adsorption.[40] The structural properties of the adsorbed NPcat layer were obtained from both QCM-D and SPR data. QCM-D showed high dissipation factors ($\Delta D > 15 \times 10^{-6}$), indicating that the adsorbed layer was soft, viscoelastic, and water-swollen (Figure 1C). Therefore, a Voigt viscoelastic model[41] was used to calculate the adsorbed mass and to determine its viscoelastic properties (Table 1). Figure 1E shows the obtained changes in mass during NPcat adsorption. The adsorbed amount measured by QCM-D and SPR corresponded to 28 and 13 mg m^{-2}, respectively. Noteworthy, QCM-D is an electroacoustic technique that measures the shift in wet mass, e.g., it accounts for the solvent coupled to the adsorbed molecules (the nanogel layer). In contrast, SPR measures the changes in refractive index at the sensor's surface, which are directly related to the effectively adsorbed mass.[42] Since there is no difference between the refractive index of the water medium and that of hydration water, the SPR signal does not track with changes in hydration. Consequently, a water content (m_{water}/m_{solid}) of 118% in the adsorbed NPcat layer can be estimated by comparing the results from QCM (wet mass, including coupled water) and SPR (effective mass). This equals a layer solid content of 46 wt%. In addition, the differences in layer thickness measured with QCM-D and SPR (Figure 1F) further confirm that the nanogel layer was highly hydrated.

The AFM height profile and phase image of NPcat adsorbed on CNF (**Figure 2**) indicate that the substrate was covered homogeneously, but since the AFM imaging was conducted in a dry/deswollen state, it naturally underestimates the difference.

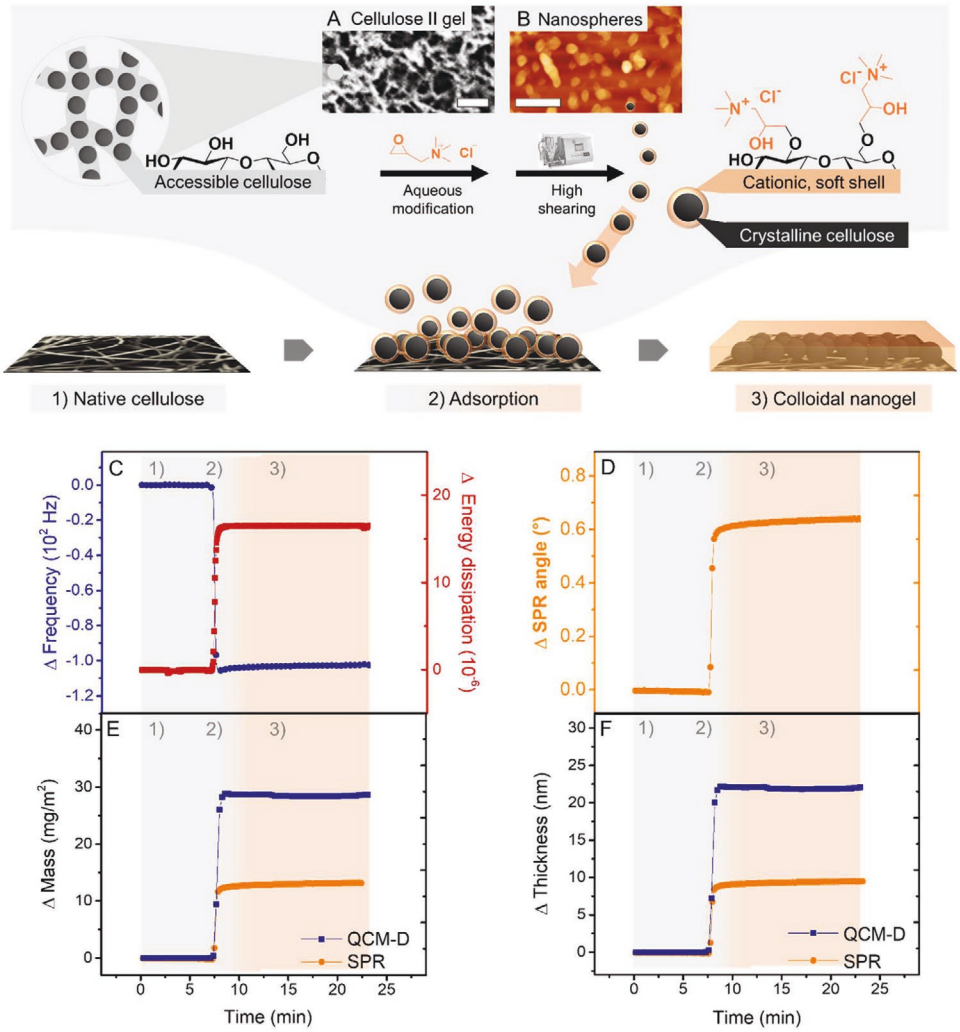

Figure 1. A nanostructured cellulose II gel (A) is further processed by aqueous cationization and subsequent mechanical shearing to yield soft cellulose II nanospheres (B) comprising an amorphous shell and a crystalline core. The introduction of cationic groups into the amorphous, accessible cellulose regions weakens interparticle interactions and allows individualization into cellulose II nanoparticles, as shown by atomic force microscope imaging (A,B 100 nm scale bar). C,D) The adsorption of the soft cationic cellulose II nanospheres onto thin films of cellulose nanofibrils was monitored with quartz crystal microbalance (QCM-D) and surface plasmon resonance (SPR). High dissipation factors measured upon adsorption indicated that the introduced colloidal nanogel layer was soft and viscoelastic. E,F) Comparison of layer mass and thickness from SPR and QCM-D were rationalized in terms of a highly water-swollen layer.

The soft cellulose II nanospheres core feature size of ≈16 nm,[12] which lies in between the thickness values from QCM-D (22 nm) and SPR (10 nm). Most likely, NPcat forms a colloidal monolayer onto the CNF surface, which is jammed through particle flattening and interparticle interpenetration. Analysis of the QCM-D with the Voigt viscoelastic model revealed further the pronounced viscoelastic properties of the NPcat layer, featuring an elastic shear modulus of ≈170 kPa (Table 1). Compared to rheological data,[12] this would equal the storage modulus of a cellulose II nanosphere dispersion at ≈10 wt%. We compared the adsorption of NPcat with that of a soluble polymer with the same cationic functional group (cationic starch) (Figure S4, Supporting Information, and Table 1). The frequency shift upon adsorption, Δf, was more than fivefold lower. Similarly, the shift in dissipation, ΔD, was also less pronounced in the latter case ($\Delta f = -17.7$ Hz and $\Delta D = 5 \times 10^{-6}$).

Table 1. Properties of the adsorbed cationic layers onto thin films, obtained from QCM-D data with the Voigt viscoelastic model.

Sample	$m_{Sauerbrey}$[a)] [mg m^{-2}]	m_{Voigt} [mg m^{-2}]	Elastic shear modulus [kPa]	Viscosity [mPa s]	Thickness [nm]
Soft colloid (NPcat)	19.2	28.4	173	1.84	21.9
Soluble polymer	3.15	10.1	46.4	1.00	7.3

[a)]The $m_{Sauerbrey}$ obtained by using Sauerbrey equation[43] is given as comparison.

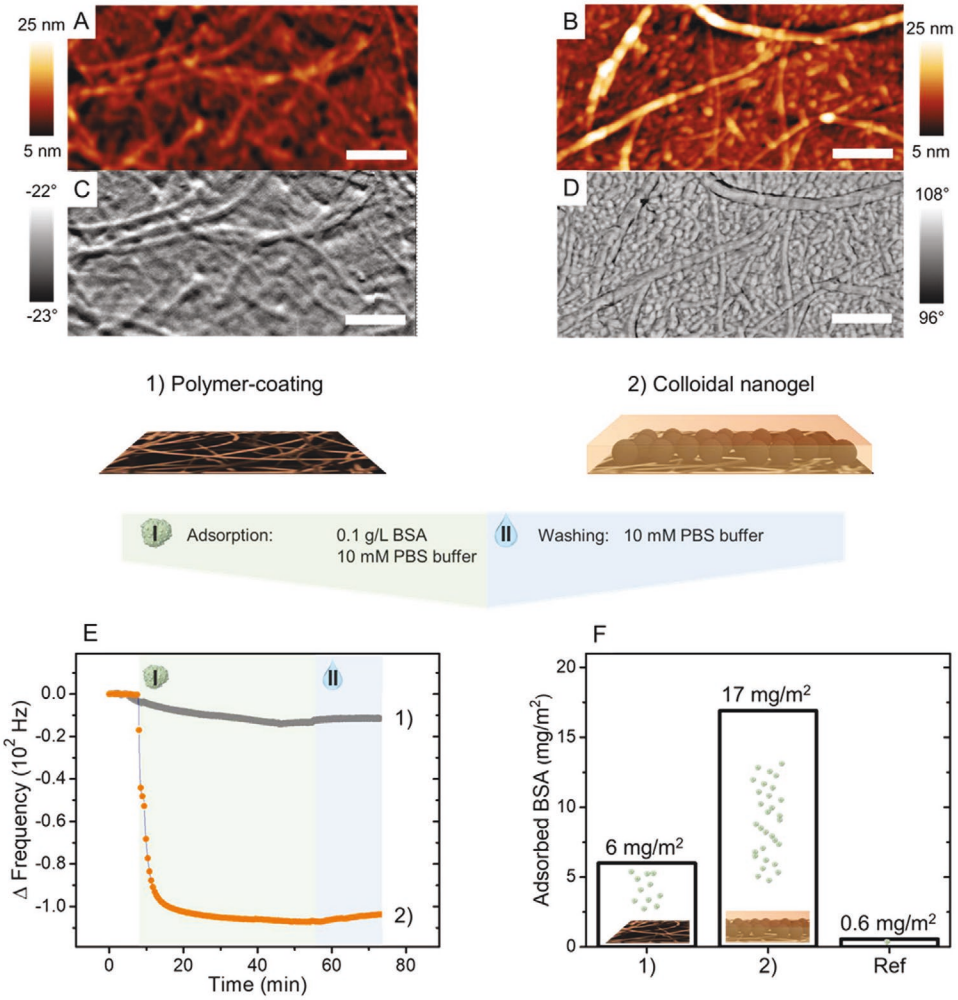

Figure 2. Comparison of native cellulose thin film surface before (A,C) and after adsorption of the colloidal nanogel (B,D) by AFM analysis in the dry state (500 nm scale bar). Nonspecific protein affinity of coated and pristine surfaces to negatively charged BSA monitored by microgravimetry: BSA adsorption on 1) a polymer coating (cationic starch) (E1 and F1), 2) colloidal nanogel (E2 and F2) with pristine cellulose as reference (F, Ref). F) The BSA adsorbed amounts suggest a remarkably enhanced protein affinity to the NPcat nanogel layer.

This is expected, since water-soluble cationic starch only adsorbs on the accessible CNF surface and structural voids.

In the next phase of the study, NPcat deposited on cellulose surfaces was used to investigate protein interactions. Here, we demonstrate the ability of NPcat to improve both nonspecific and specific protein adsorption. First, interactions of a negatively charged protein and previously adsorbed positively charged layers were observed in QCM-D. BSA adsorption on NPcat-supported nanogel layer, soluble polymer-coating (cationic starch) on CNF and pristine CNF (reference) were compared in Figure 2E,F. Noteworthy, BSA was negatively charged at the testing conditions (pH 7.4), given its isoelectric pH of 4.7.[44] Therefore, due to electrostatic repulsion, only minor adsorption of BSA was measured on the reference CNF surface (Figure S5A, Supporting Information). In contrast, the surfaces modified with cationic materials adsorbed BSA (Figure 2E). However, the adsorption capability of the NPcat nanogel layer was significantly higher compared to that of the polymer-coated CNF substrate. Adsorbed protein amounts were calculated using the Voigt viscoelastic model, and 17, 6.0, and 0.57 mg m^{-2} were obtained for NPcat layer, cationic starch polymer-coating, and pristine CNF, respectively (Figure 2F). The results of the last two are comparable to literature values for BSA adsorption onto cationic cellulose or chitosan surfaces (0.6–4.5 mg m^{-2})[28,31,33,45] and native cellulose (0.2–0.9 mg m^{-2})[28,29,31,46] under similar conditions. Furthermore, the BSA adsorption onto NPcat turns out to be significantly higher, even compared to polydimethylsiloxane and polyethyleneimine (7 and 9 mg m^{-2}, respectively), which are commonly used layers for immunoactive reagent immobilization.[47] Comparison to these literature values also shows that although cationic starch has a lower degree of substitution than NPcat (0.05 vs 0.17), it is a very good reference as cationic polymer coating. The studied cationic starch had a similar polymer adsorption than that of higher charged cationic polymers, such as cationic cellulose, chitosan, and polyethyleneimine.[28,31,33,45,47]

The BSA affinity to the NPcat nanogel layer was remarkably enhanced. Usually, the repulsive double layer forces of individual, negatively charged BSA[35] limit protein adsorption,

Table 2. Properties of the adsorbed protein layers, obtained with the Voigt viscoelastic modeling from the QCM-D data. The $m_{Sauerbrey}$ obtained by using the Sauerbrey equation[43] is given as a comparison.

Sample	$m_{Sauerbrey}$ [mg m^{-2}]	m_{Voigt} [mg m^{-2}]	Elastic shear modulus [kPa]	Viscosity [mPa s]	Thickness [nm]
Reference	0.35	0.57	23.2	0.26	0.48[a)]
Soft colloid (NPcat)	17.4	16.9	547	3.95	12.9
Soluble polymer	2.4	6.01	57.6	1.00	4.3

[a)]Value indicates that the adsorbed layer is not fully covering the CNF film since the Stokes radius of BSA is 3.5 nm.[48]

but the pronounced adsorption on the nanogel layer, as well as the considerable increase in the elastic shear moduli, from 173 to 547 kPa, and layer viscosity, from 2 to 4 mPa s (Tables 1 and **2**), all point to the fact that BSA penetrated the colloidal nanogel, stiffening the associated physical network.

In general, protein adsorption is preferentially conducted at a pH close to its isoelectric point, to avoid repulsive double-layer interactions;[35] hence, we investigated the nonspecific adsorption of neutral hIgG on cellulose filter papers (hereafter referred as paper) using confocal laser scanning microscopy (CLSM). Human IgG (hIgG) antibodies were chosen for this study since they are important recognition elements in diagnostic tools, e.g., to indicate the immune status of patients exposed to pathogens, such as hepatitis B and measles viruses.[49] In this study, hIgG antibodies labeled with a fluorescent tag (hIgG-FITC) were adsorbed on paper carrying a NPcat gel layer on its surface (**Figure 3**B). Results for paper covered with a soluble polymer-coating (Figure 3A) are also shown. For comparison of the different samples, the relative fluorescence intensity was determined by image analyses (Table S2, Supporting Information). The reference paper did not adsorb hIgG-FITC to a significant extent with a relative fluorescence intensity of only 2.2 (Figure 3 Ref).

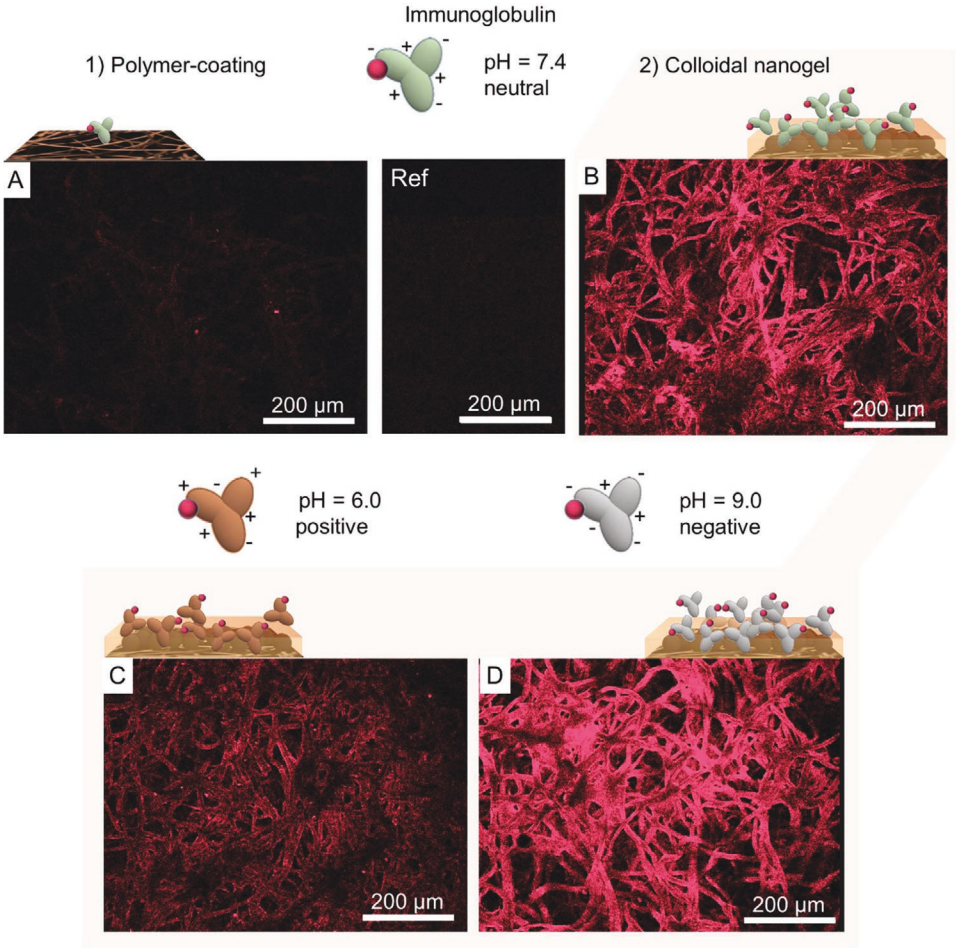

Figure 3. Surface functionalization of BSA-blocked filter paper substrates to enhance nonspecific adsorption of fluorescent-labeled human immunoglobulin G: Confocal microscopy images of adsorbed antibody onto paper support coated with a cationic polymer (A) and colloidal nanogel (B) are compared to the bare paper reference (Ref). The colloidal nanogel layer offers a highly accessible surface and a significantly improved protein affinity. C,D) This higher affinity is also achieved when the net charge of immunoglobulin is positive or negative.

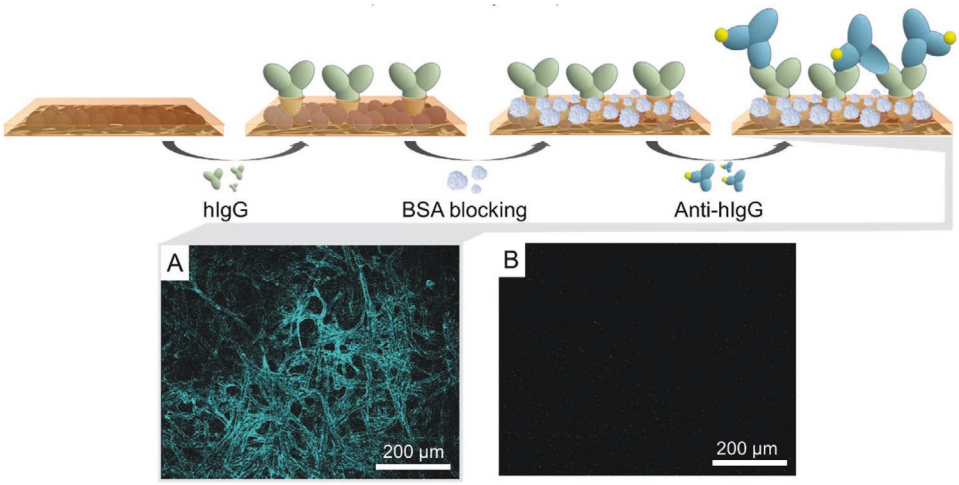

Figure 4. Immobilization of a colloidal nanogel layer onto paper enabled specific antibody–antibody interactions. Schematic illustration of the three-step adsorption process: 1) Immunoglobulin (hIgG) was adsorbed on the nanogel layer. 2) Bovine serum albumin (BSA) was used as a blocking molecule for nonspecific binding sites, and 3) fluorescent-tagged anti-hIgG was adsorbed specifically to hIgG. The adsorption of the tagged anti-hIgG onto the colloidal nanogel layer (A) and the reference paper (B) was monitored by confocal microscopy.

Furthermore, only a weak fluorescence signal (intensity ≈2.8) was detected on the sample carrying the polymer-coated layer, demonstrating minor antibody adsorption (Figure 3A). In contrast, a high fluorescence (intensity ≈27.9) was observed from images of paper carrying a NPcat layer, indicating a high affinity of the antibody to the nanoparticles (Figure 3B). Since there are multiple human IgG subclasses, no single isoelectric point can be assigned to hIgG, but reported to be in the range of pH between 6.6 and 8.2.[50] Consequently, the net charge of the hIgG was estimated to be close to neutral at pH 7.4, and therefore, adsorption was mainly driven by nonelectrostatic forces. Thus, adsorption of hIgG occurred most likely due to van der Waals interactions, and/or the entropy gain caused by solvent molecule or counterion release.[51] However, despite the net zero overall charge of the protein at the isoelectric point, there are still charged domains on the surface, which drive electrostatic interactions.[40] Consequently, it is possible that adsorption of hIgG antibodies occurred via the exposed, oppositely charged NPcat surfaces. This behavior and the other nonelectrostatic interactions explain why net positively charged hIgG was adsorbed to surfaces with the same charge, i.e., at conditions below its isoelectric point range.[51] Namely, adsorption of hIgG-FITC on NPcat was also detected at pH 6 (hIgG positively charged) and at pH 9 (hIgG negatively charged) (Figure 3C,D). The fluorescence intensity values of 13.5 and 38.0 were obtained from the images taken at pH 6 and pH 9, respectively. Furthermore, the NPcat had higher affinity to the antibody at pH 6 and 9 compared to the soluble polymer-coating (fluorescence intensity ≈6.2 and 5.1 at pH 6 and pH 9, respectively) (Figure S6, Supporting Information), showing that NPcat surfaces could be employed to increase sensitivities of state-of-the-art antibody tests based on polymer-coated surfaces.

Besides, the enhanced adsorption ability of NPcat-modified paper compared to unmodified and polymer-coated papers was also demonstrated in tests with anionic fluorescein sodium salt. The differences in sample adsorption capabilities could be seen with the naked eye (Figure S7, Supporting Information). This demonstrates that the application of NPcat-modified surfaces for adsorption-related processes is broad and not restricted to diagnostics.

In order to determine whether the NPcat nanogel layer facilitates specific protein interactions, adsorption tests were performed with hIgG antibodies and fluorescent-stained anti-human IgG (anti-hIgG) antibodies on papers and analyzed via CLSM. **Figure 4** illustrates three-step adsorption of antibodies on the NPcat nanogel layer: 1) hIgG antibodies were adsorbed nonspecifically on the NPcat layer. 2) The remaining nonspecific adsorption sites were blocked with blocker molecules (BSA), and 3) the fluorescent-tagged anti-antibody (anti-hIgG-FITC) was bound specifically to hIgG. This kind of antibody–antibody interaction is employed, for example, in indirect immunoassays, where a primary antibody is used in antigen detection and a secondary antibody produces a detectable signal.[52]

Confocal images show the specific interaction of anti-hIgG-FITC with hIgG adsorbed onto the colloidal nanogel layer-decorated paper (Figure 4A), in comparison to the reference paper (Figure 4B). The obtained dark (black) images of the reference paper show that in the case of the sample without hIgG antibodies, no anti-hIgG antibodies adsorption occurred (fluorescence intensity ≈2.7, Table S3, Supporting Information). The image of the colloidal nanogel paper with physically bound antibodies shows intensive fluorescence (intensity ≈19.6), indicating significant binding of the anti-antibody. The interactions were specific since nonspecific binding sites were blocked with BSA prior to imaging.

3. Conclusions

NPcat were produced from a cellulose II hydrogel by aqueous cationization and subsequent mechanical shearing. NPcat, with a hydrodynamic radius of 55 nm, showed an intrinsic solid core/soft shell structure. Adsorption of these colloids onto an oppositely charged cellulose surface was monitored by

microgravimetry and surface plasmon resonance. The cellulose surface was homogeneously covered with NPcat, forming a viscoelastic and water-swollen colloidal nanogel layer. The interaction of this layer with differently charged proteins was compared to a traditional polymer-based coating, revealing a significantly higher affinity of proteins to the colloidal nanogel. The formed accessible gel layer on cellulose had not only substantial affinity to nonspecific proteins in a broad pH range but could be also used as an anchoring layer for specific protein interactions. The capability of the colloidal nanogel to facilitate protein interactions reveals its potential as an anchor layer for adsorption-related processes, offering a powerful alternative to state-of-the-art polymer-coatings with a high potential to overcome the current sensitivity limitations of immunosensors.

4. Experimental Section

Materials: The cellulose II gel also referred to as LENZING(TM) lyocell gel[11,36] ((LENZING(TM) is a trademark of Lenzing AG) with a solid content of 4 wt% was provided by Lenzing AG and stored at 8 °C until use. Cellulose nanofibril (CNF) suspension (1.48 wt%) was prepared from bleached sulfite birch fibers (12 passes through a M110P fluidizer (Microfluidics Corp.)). Cationic starch (Raisamyl 150) with a degree of substitution of 0.05 was purchased from Chemigate. Cationic starch was used as an example for a soluble cationic polymer. Dimethyl sulfoxide (DMSO) (≥99.9%) was purchased from Merck. D_2SO_4 and D_2O were obtained from Euriso-top. All other chemicals were purchased from Sigma-Aldrich (Finland): Fluorescein 5(6)-isothiocyanate (FITC) (≥90%), polyethyleneimine (PEI) 50% aqueous solution (M_w 600 000–1 000 000 g mol^{-1}), glycidyltrimethylammonium chloride (20–25% water, dry substance ≥90%, techn.), hIgG (≥95%), anti-hIgG γ-chain specific antibody produced in rabbit, and BSA (≥98%). Water purified with a Millipore Synergy UV unit (Milli-Q) was used.

Preparation of Cellulose II Nanoparticles: The cellulose II gel was concentrated at 10 000 rcf for 10 min to a solid content of 9.2 wt%. 32 g of this material (2.95 g of dry cellulose, 18.2 mmol) was transferred into a 100 mL Schott bottle. The suspension was mixed with a glass rod due to its high viscosity and a 50 wt% aqueous solution of NaOH (0.38 g, 4.8 mmol) was added slowly while mixing. After 30 min, glycidyl trimethylammonium chloride (5.5 mL, 6.2 g, 29.5 mmol (considering 90% purity and a water content of 20%), 1.6 eq) was added and the highly viscous gel was homogeneously mixed with a glass rod and transferred into a water bath shaker at 55 °C. After 20 h, 60 mL of Milli-Q water was added, and the suspension was washed with Milli-Q water following three washing and centrifugation cycles (5 min@10 000 rcf). The suspension was further purified by dialysis (6–8 kDa regenerated cellulose membrane) against deionized water for 4 d. Finally, the suspensions were homogenized in a microfluidizer (Microfluidics M110P, Microfluidics Corporation, USA) (2 passes@2000 bar) to yield individualized spherical nanoparticles. The degree of substitution of 0.17 was determined by liquid-state NMR from a hydrolyzed NPcat sample, the particles were further analyzed by small-angle X-ray scattering as well as dynamic and electrophoretic light scattering (see the Supporting Information for more details). The number of cationic surface groups of NPcat was calculated from the degree of substitution and corresponds to 0.9 mmol g^{-1}.

Atomic Force Microscopy: The surface topography of the particles was studied on SiO_2 wafers or QCM sensors by a Nanoscope IIIa multimode scanning probe microscope (Digital Instruments, USA). Surface areas of 3×3 and 1×1 μm^2 were investigated in air using tapping mode with silicon cantilevers (NSC15/ALBS, MikroMasch, 8 nm tip radius). Images were processed (flattening) and analyzed with Gwyddion software.

Preparation of CNF Model Surfaces: Ultrathin films of CNF were prepared as described by Ahola et al.[53] First, 0.148% CNF suspension was defibrillated with a tip sonicator (Digital Sonifier Model 450, Barbson Ultrasonics Corp.) for 10 min at 25% amplitude. Then, CNF suspension was centrifuged at 10 000 rcf for 45 min. The supernatant with individual nanofibrils was collected with a pipette. Then, the nanofibrils from the supernatant were spin-coated (Model WS-650SX-6NPP, Laurell Technologies) at 3000 rpm onto UV-ozonized QCM sensors (QSX 301, Q-sense) and SPR sensors (SPR102-AU, BioNavis) with a thin anchor layer of cationic PEI. Finally, the spin-coated substrates were dried in an oven at 80 °C for 10 min.

Quartz Crystal Microbalance with Dissipation Monitoring: QCM-D (E4 instrument, Q-Sense AB) was utilized to monitor adsorption of charged materials on thin CNF films and sequential adsorption of BSA (0.1 g L^{-1}) on these surfaces at pH 7.4. Phosphate buffer (pH 7.4, 10×10^{-3} M) was used for film equilibration and as washing buffer. Changes in the sensor oscillation frequency were measured at a fundamental resonance frequency of 5 MHz. All measurements were performed at 23 °C under the constant flow of 100 μL min^{-1}. The adsorbed masses were calculated with the Sauerbrey equation (Equation (1))

$$\Delta m = -C_{\mathrm{QCM}} \frac{\Delta f}{n} \tag{1}$$

where C_{QCM} is 17.7 ng Hz^{-1} cm^{-2} for 5 MHz crystal, Δf is the change in frequency, and n is the overtone number.[43,54] However, the Sauerbrey equation is not usually suitable for mass estimations if the adsorbed layer is not rigid.[55] Therefore, also the Voigt viscoelastic model (Q-Tools software, version 2.1 Q-Sense) was used to estimate the adsorbed masses (see Figure S8, Supporting Information, showing typical fittings to the thickness of adsorbed layers via Voigt viscoelastic model). The fluid density was approximated to 1000 kg m^{-3}, the fluid viscosity to 0.001 m^3 kg^{-1}, and the density of the adsorbed layers to be 1300 kg m^{-3}.

Adsorption of Charged Materials and Protein on CNF Model Surfaces in QCM-D: Prior measurements, CNF films were placed inside QCM chambers and stabilized in a phosphate buffer (pH 7.4, 10×10^{-3} M) until a stable baseline was observed. After stabilization, 0.5 wt% NPcat or 0.5 wt% cationic starch were adsorbed on CNF films for 20 min. Then, loosely bound particles were removed by washing with the buffer for 15 min. Next, 0.1 g L^{-1} BSA (in phosphate buffer, pH 7.4) was adsorbed on the pristine CNF surface and the NPcat- and starch-modified CNF surfaces for 50 min. Finally, washing with the buffer was done for 20 min.

Surface Plasmon Resonance: Multiparametric SPR instrument (MP-SPR Model Navi 200, Oy BioNavis Ltd.) was used to monitor adsorption of NPcat on thin CNF films. All SPR measurements were performed at 20 °C under the constant flow of 100 μL min^{-1}. The thickness of the adsorbed layer was determined with Equation (2)[56]

$$d = \frac{l_d}{2} \frac{\Delta_{\mathrm{angle}}}{m(n_a - n_0)} \tag{2}$$

where d is the thickness, l_d is the characteristic evanescent electromagnetic field decay length (estimated as 0.37 of the light wavelength 670 nm), Δ_{angle} is the change in the SPR angle, m is the sensitivity factor for the sensor (109.94° RIU^{-1}, obtained after calibration), n_0 is the refractive index of the bulk solution (1.334 RIU), and n_a is the refractive index of the adsorbed substance (for NPcat 1.410[57]).

The mass of the adsorbed layer per unit area was determined with Equation (3)[58]

$$\Delta m = d \times \rho \tag{3}$$

where Δm is the adsorbed mass, d is the thickness, and ρ is the packing density of the NPcat (estimated to be 1.39 g cm^{-3}[57]).

Adsorption of NPcat on CNF Model Surfaces in SPR: Prior measurements, CNF films were placed inside SPR and stabilized in a phosphate buffer (pH 7.4, 10×10^{-3} M) until a stable baseline was observed. After stabilization, 0.5 wt% NPcat were adsorbed on CNF films for 80 min. Then, loosely bound particles were removed by washing with the buffer for 40 min.

Fluorescein Labeling of hIgG and Anti-hIgG: To modify antibodies with a fluorescent probe, a procedure for immunoglobulin modification by Hermanson[59] was used with few alterations. First, 2 mg mL^{-1} protein

solution was prepared in 0.1 M sodium carbonate buffer (pH 9.0). Then, 1 g L^{-1} FITC solution was prepared in a dark room by dissolving FITC in dry DMSO. This solution was protected from light by wrapping the sample container in aluminum foil. Next, 100 µL of the FITC solution was added dropwise to each ml of hIgG solution and gently mixed. The reaction occurred at 4 °C for 8 h. To purify the obtained FITC-stained hIgG (hIgG-FITC) and anti-hIgG (anti-hIgG-FITC) from unreacted FITC molecules, the solution was centrifuged four times at 3500 rcf for 30 min by using centrifugal filter units (Amicon Ultra-15, MWCO 30 kDa).

Nonspecific Protein Adsorption and CLSM: Nonspecific adsorption behavior of hIgG-FITC was studied on filter papers. First, paper substrates were immersed in a 5 wt% BSA solution for 10 min in order to block the surfaces. Then, 30 µL of 1 wt% cationic starch or 1 wt% NPcat were adsorbed on the BSA-blocked substrates. Finally, 30 µL of 0.1 g L^{-1} hIgG-FITC (in 10×10^{-3} M phosphate buffer (pH 6 or 7.4) or sodium carbonate buffer (pH 9)) was adsorbed on the samples. Additionally, 10 min washing with buffer (pH 6, 7.4, or 9) and drying with N_2 gas were done after each adsorption step. Then, the hIgG-FITC exposed samples were imaged with CLSM to detect the adsorbed antibodies. Images were taken with a laser scanning spectral confocal microscope (Leica TCS SP2, Leica microsystems CMS GmbH) by using 488 nm excitation wavelength and 500–540 nm detection wavelength range. Images were acquired with 848 V laser power and under constant imaging conditions. After imaging, the intensity of the fluorescence images was measured using the color analysis tool of the GNU Image Manipulation Program. The intensity was measured from the unmodified images (Table S2, Supporting Information).

Specific Protein Adsorption and CLSM: First, 1 wt% NPcat was physically adsorbed on BSA-blocked filter papers for 10 min. Then, 30 µL of 0.1 g L^{-1} hIgG (in 10×10^{-3} M phosphate buffer, pH 7.4) was adsorbed on the samples. Next, samples were blocked by immersing them in a 5 wt% BSA solution for 10 min. Then, 30 µL of 0.1 g L^{-1} anti-hIgG-FITC (in 10×10^{-3} M phosphate buffer, pH 7.4) was adsorbed on the samples for 10 min. Additionally, 10 min washing step with a phosphate buffer (pH 7.4, 10×10^{-3} M) and drying with N_2 gas were done after each adsorption step. To determine if the anti-antibodies bound with the antibody on the paper samples, all samples were imaged with CLSM (Leica TCS SP2, Leica microsystems CMS GmbH). 488 nm excitation wavelength and 500–540 nm detection wavelength range were used. Images were acquired with 848 V laser power and under constant imaging conditions. After imaging, the intensity of the fluorescence images was measured using the color analysis tool of the GNU Image Manipulation Program. The intensity was measured from the unmodified images (Table S3, Supporting Information).

Supporting Information

Supporting Information is available from the Wiley Online Library or from the author.

Acknowledgements

This project received funding from the European Union's Horizon 2020 research and innovation programme under Grant Agreement No. 760876 and the ERC Advanced Grant Agreement No. 788489, "BioElCell." This work was also part of the Academy of Finland's Flagship Programme under Project Nos. 318890 and 318891 (Competence Center for Materials Bioeconomy, FinnCERES). K.S. acknowledges funding by the Aalto University School of Chemical Engineering doctoral programme. The Canada Excellence Research Chair initiative is gratefully acknowledged (O.J.R.).

Conflict of Interest

The authors declare no conflict of interest.

Author Contributions

K.S. and M.B. contributed equally to this work. The manuscript was written through the contributions of all authors. All authors have given approval to the final version of the manuscript.

Keywords

amorphous nanocellulose, cellulose II nanogel, colloids, core/shell nanoparticles, immunosensors, protein adsorption

Received: August 3, 2020
Revised: October 20, 2020
Published online:

[1] T. Nishino, K. Takano, K. Nakamae, *J. Polym. Sci., Part B: Polym. Phys.* **1995**, *33*, 1647.
[2] I. Diddens, B. Murphy, M. Krisch, M. Müller, *Macromolecules* **2008**, *41*, 9755.
[3] Y. Habibi, L. A. Lucia, O. J. Rojas, *Chem. Rev.* **2010**, *110*, 3479.
[4] K. Chatterjee, S. Sarkar, K. J. Rao, S. Paria, *Adv. Colloid Interface Sci.* **2014**, *209*, 8.
[5] M. B. Gawande, A. Goswami, T. Asefa, H. Guo, A. V. Biradar, D. L. Peng, R. Zboril, R. S. Varma, *Chem. Soc. Rev.* **2015**, *44*, 7540.
[6] J. O. Zoppe, Y. Habibi, O. J. Rojas, R. A. Venditti, L. S. Johansson, K. Efimenko, M. Österberg, J. Laine, *Biomacromolecules* **2010**, *11*, 2683.
[7] J. Majoinen, A. Walther, J. R. McKee, E. Kontturi, V. Aseyev, J. M. Malho, J. Ruokolainen, O. Ikkala, *Biomacromolecules* **2011**, *12*, 2997.
[8] L.-Q. Zhang, B. Niu, S.-G. Yang, H.-D. Huang, G.-J. Zhong, Z.-M. Li, *ACS Sustainable Chem. Eng.* **2016**, *4*, 2470.
[9] H. Q. Wang, H. Tan, S. Hua, Z. Y. Liu, W. Yang, M. B. Yang, *Macromol. Rapid Commun.* **2017**, *38*, 1700409.
[10] M. Beaumont, H. Rennhofer, M. Opietnik, H. C. Lichtenegger, A. Potthast, T. Rosenau, *ACS Sustainable Chem. Eng.* **2016**, *4*, 4424.
[11] M. Beaumont, T. Nypelö, J. König, R. Zirbs, M. Opietnik, A. Potthast, T. Rosenau, *Green Chem.* **2016**, *18*, 1465.
[12] M. Beaumont, S. Rosenfeldt, B. L. Tardy, C. Gusenbauer, A. Khakalo, Nonappa, M. Opietnik, A. Potthast, O. J. Rojas, T. Rosenau, *Nanoscale* **2019**, *11*, 17773.
[13] J. Zhang, T. J. Elder, Y. Pu, A. J. Ragauskas, *Carbohydr. Polym.* **2007**, *69*, 607.
[14] M. Cheng, Z. Qin, Y. Liu, Y. Qin, T. Li, L. Chen, M. Zhu, *J. Mater. Chem. A* **2014**, *2*, 251.
[15] C. F. Yan, H. Y. Yu, J. M. Yao, *Cellulose* **2015**, *22*, 3773.
[16] M. Beaumont, A. Kondor, S. Plappert, C. Mitterer, M. Opietnik, A. Potthast, T. Rosenau, *Cellulose* **2017**, *24*, 435.
[17] D. Vlassopoulos, M. Cloitre, *Soft Matter* **2012**, *8*, 4010.
[18] G. M. Conley, P. Aebischer, S. Nöjd, P. Schurtenberger, F. Scheffold, *Sci. Adv.* **2017**, *3*, e1700969.
[19] N. Gnan, E. Zaccarelli, *Nat. Phys.* **2019**, *15*, 683.
[20] A. V. Kabanov, S. V. Vinogradov, *Angew. Chem., Int. Ed.* **2009**, *48*, 5418.
[21] C. Zhao, Q. Chen, K. Patel, L. Li, X. Li, Q. Wang, G. Zhang, J. Zheng, *Soft Matter* **2012**, *8*, 7848.
[22] L. A. Tessler, C. D. Donahoe, D. J. Garcia, Y. S. Jun, D. L. Elbert, R. D. Mitra, *J. R. Soc., Interface* **2011**, *8*, 1400.
[23] J. R. Clegg, C. M. Ludolph, N. A. Peppas, *J. Appl. Polym. Sci.* **2020**, *137*, 48655.
[24] C. Zhao, K. Patel, L. M. Aichinger, Z. Liu, R. Hu, H. Chen, X. Li, L. Li, G. Zhang, Y. Chang, J. Zheng, *RSC Adv.* **2013**, *3*, 19991.
[25] F. Rusmini, Z. Zhong, J. Feijen, *Biomacromolecules* **2007**, *8*, 1775.

[26] H. D. Dhruv, *Controlling Nonspecific Adsorption of Proteins at Bio-Interfaces for Biosensors and Biomedical Applications*, Utah State University, Logan, UT **2009**.
[27] M. A. Cole, N. H. Voelcker, H. Thissen, H. J. Griesser, *Biomaterials* **2009**, *30*, 1827.
[28] H. Orelma, I. Filpponen, L. S. Johansson, J. Laine, O. J. Rojas, *Biomacromolecules* **2011**, *12*, 4311.
[29] K. Solin, H. Orelma, M. Borghei, M. Vuoriluoto, R. Koivunen, O. J. Rojas, *Biomacromolecules* **2019**, *20*, 1036.
[30] S. Lombardo, S. Eyley, C. Schütz, H. Van Gorp, S. Rosenfeldt, G. Van Den Mooter, W. Thielemans, *Langmuir* **2017**, *33*, 5473.
[31] T. Mohan, K. Niegelhell, C. S. P. Zarth, R. Kargl, S. Köstler, V. Ribitsch, T. Heinze, S. Spirk, K. Stana-Kleinschek, *Biomacromolecules* **2014**, *15*, 3931.
[32] M. Vuoriluoto, H. Orelma, B. Zhu, L. S. Johansson, O. J. Rojas, *ACS Appl. Mater. Interfaces* **2016**, *8*, 5668.
[33] T. Mohan, T. Ristić, R. Kargl, A. Doliska, S. Köstler, V. Ribitsch, J. Marn, S. Spirk, K. Stana-Kleinschek, *Chem. Commun.* **2013**, *49*, 11530.
[34] P. D. Ross, S. Subramanian, *Biochemistry* **1981**, *20*, 3096.
[35] S. H. Lee, E. Ruckenstein, *J. Colloid Interface Sci.* **1988**, *125*, 365.
[36] J. Männer, M. Opietnik, J. Innerlohinger, G. Reiter, M. Hager, WO/2015/054712 **2015**.
[37] N. Odabas, H. Amer, M. Bacher, U. Henniges, A. Potthast, T. Rosenau, *ACS Sustainable Chem. Eng.* **2016**, *4*, 2295.
[38] H. Liimatainen, M. Visanko, J. A. Sirviö, O. E. O. Hormi, J. Niinimaki, *Biomacromolecules* **2012**, *13*, 1592.
[39] K. P. Y. Shak, Y. L. Pang, S. K. Mah, *Beilstein J. Nanotechnol.* **2018**, *9*, 2479.
[40] S. T. Moerz, P. Huber, *Langmuir* **2014**, *30*, 2729.
[41] M. V. Voinova, M. Rodahl, M. Jonson, B. Kasemo, *Phys. Scr.* **1999**, *59*, 391.
[42] J. Malmström, H. Agheli, P. Kingshott, D. S. Sutherland, *Langmuir* **2007**, *23*, 9760.
[43] G. Sauerbrey, *Z. Phys.* **1959**, *155*, 206.
[44] C. Chaiyasut, T. Tsuda, *Chromatography* **2001**, *22*, 91.
[45] X. Xu, C. Zhang, Y. Zhou, Q. L. J. Cheng, K. Yao, Q. Chen, *J. Bioact. Compat. Polym.* **2007**, *22*, 195.
[46] Y. Zhang, R. G. Carbonell, O. J. Rojas, *Biomacromolecules* **2013**, *14*, 4161.
[47] T. Mohan, A. Čas, M. Bračič, O. Plohl, A. Vesel, M. Rupnik, L. F. Zemljič, J. Rebol, *ACS Biomater. Sci. Eng.* **2019**, *5*, 5825.
[48] I. Axelsson, *J. Chromatogr. A* **1978**, *152*, 21.
[49] T. Shors, *Understanding Viruses*, Jones & Bartlett Publishers, Burlington, MA **2011**.
[50] D. Yang, R. Kroe-Barrett, S. Singh, T. Laue, *Antibodies* **2019**, *8*, 24.
[51] M. Rabe, D. Verdes, S. Seeger, *Adv. Colloid Interface Sci.* **2011**, *162*, 87.
[52] S. A. Lim, M. U. Ahmed, *RSC Detection Science*, Royal Society of Chemistry, London **2019**, pp. 1–20.
[53] S. Ahola, P. Myllytie, M. Österberg, T. Teerinen, J. Laine, *BioResources* **2008**, *3*, 1315.
[54] M. Rodahl, B. Kasemo, *Sens. Actuator A Phys.* **1996**, *54*, 448.
[55] F. Höök, M. Rodahl, P. Brzezinski, B. Kasemo, *Langmuir* **1997**, *7463*, 729.
[56] L. S. Jung, C. T. Campbell, T. M. Chinowsky, M. N. Mar, S. S. Yee, *Langmuir* **1998**, *14*, 5636.
[57] C. Sampl, K. Niegelhell, D. Reishofer, R. Resel, S. Spirk, U. Hirn, *Front. Chem.* **2019**, *7*, 251.
[58] C. T. Campbell, G. Kim, *Biomaterials* **2007**, *28*, 2380.
[59] G. T. Hermanson, *Bioconjugate Techniques*, Academic, New York **2008**.